Array Signal Processing Homework, Solutions

Mordehay Moradi

August 2021

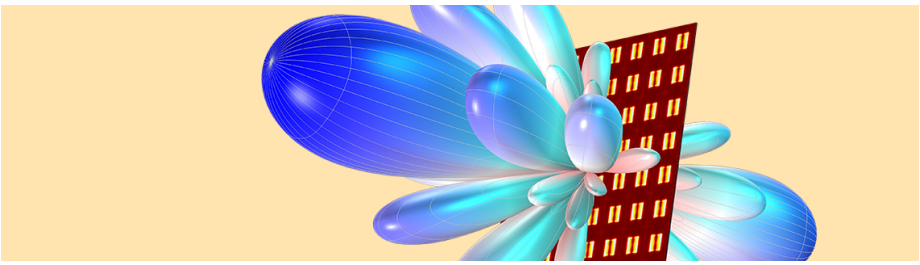

Contents

1 Beampattern of ULA

1.1

The beampattern is defined as follows:

$$B_\theta(\theta) = w^H v_\theta(\theta) = \sum_{n=0}^{N-1} w_n^* e^{j(n-n_0)\frac{2\pi d}{\lambda}\cos(\theta)} \tag{1}$$

where the value for n_0 depends on the reference point. In class we have shown that there is non-linearity in θ domain in compared with ψ domain. On the same way, we encounter the linearity of the $\cos(\theta)$ around $\theta \approx \frac{\pi}{2}[rad]$. We can see this in the following equation:

$$\psi = \frac{2\pi}{\lambda} d \cos(\theta)$$

when $\theta \approx 0$, $\cos(\theta)$ does not change much and thus we'll get more wider beam in the θ than ψ domain. However at $\theta \approx \frac{\pi}{2}[rad]$ we get more narrower beam in the θ than ψ domain. These results can be seen in figure 1.

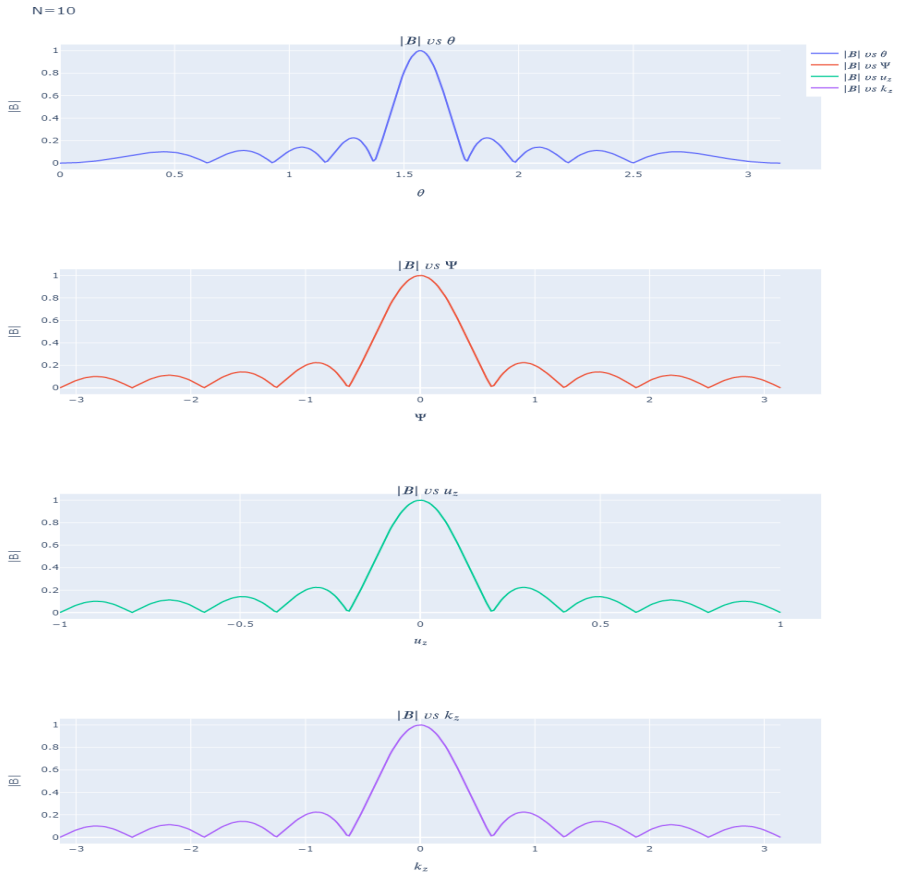

Figure 1: beam pattern in θ, ψ, k_z *and* u_z domain, N=10.

I made the graphs for the case N=11 and got the results in figure 2
As we can see in figures 1 and 2, when the number of sensors increases, we get more narrower beam. We saw this result in the class - the null to null beamwidth is given by:

$$\Delta u_2 = \frac{2\lambda}{Nd} \tag{2}$$

The ranges are:

$$k_z \in [-\frac{2\pi}{\lambda}, -\frac{2\pi}{\lambda}], \Psi \in [-\pi, \pi], u \in [-1, 1], \Theta \in [0, \pi]$$

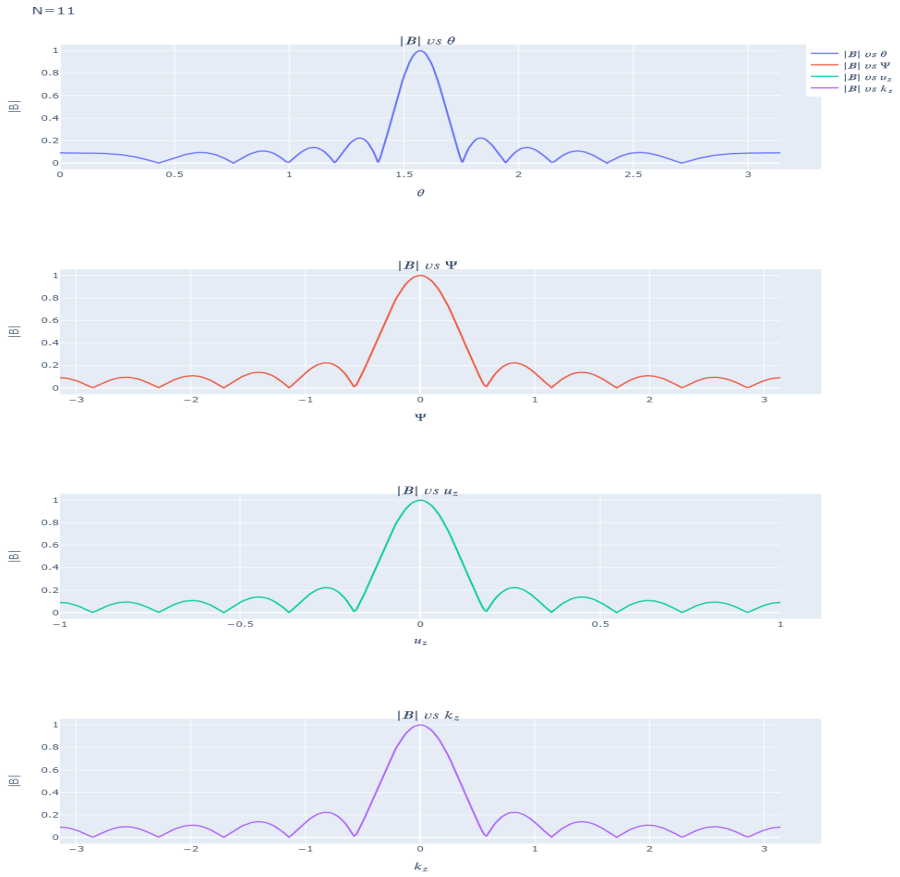

Figure 2: beam pattern in θ, ψ, k_z *and* u_z domain, N=11.

1.2

In this section we compare the polar plot of the powerpattern in the θ domain, for N=10 and N=11. The plot can be seen in figure 3
We can see from figure 3, that as the number of sensors increases the main beam is more narrower. The positions of the side lobes in the case of broadside are at $u = \pm\frac{2m+1}{2}\frac{\lambda}{Nd}$. As mentioned above $u \in [-1, 1]$, thus for $N = 10$, there are 4 sidelobes on each side of the main lobe whereas for $N = 11$ there is one more on each side

1.3

In this section we plot the powerpattern in θ domain for $0.001 \leq \frac{d}{\lambda} \leq 1$ and compare the results for broadside and endfire orientation. We can list the differences

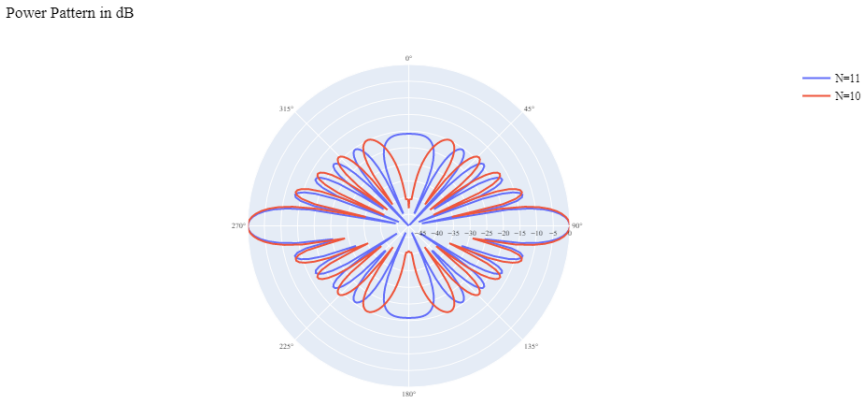

Figure 3: polar plot of the powerpattern in the θ domain.

between the plots in figure 4:

- As $\frac{d}{\lambda} \to 0$ the beam becomes more wider. The reason for this is derived from the observation the null-to-null bandwidth is proportional to $\frac{\lambda}{d}$
- The mainlobe width of the broadside is more narrower than the endfire orientation, This effect is derived from the fact that the $\cos(\theta)$ is not linear function(as I explained before)
- As we saw in class the beampattern in the angle space is given by:

$$B_\theta(\theta) = \frac{1}{N} \frac{\sin(\frac{\pi N d}{\lambda})(\cos(\theta) - \cos(\theta_T))}{\sin(\frac{\pi d}{\lambda})(\cos(\theta) - \cos(\theta_T))}$$

The grating lobes are in the visible region if:

$$-\pi \leq \frac{\pi d}{\lambda}(\cos(\theta) - \cos(\theta_T)) \leq \pi \xrightarrow[\text{for any } \theta]{} \frac{d}{\lambda} \geq \frac{1}{1 + |\cos(\theta_T)|} \tag{3}$$

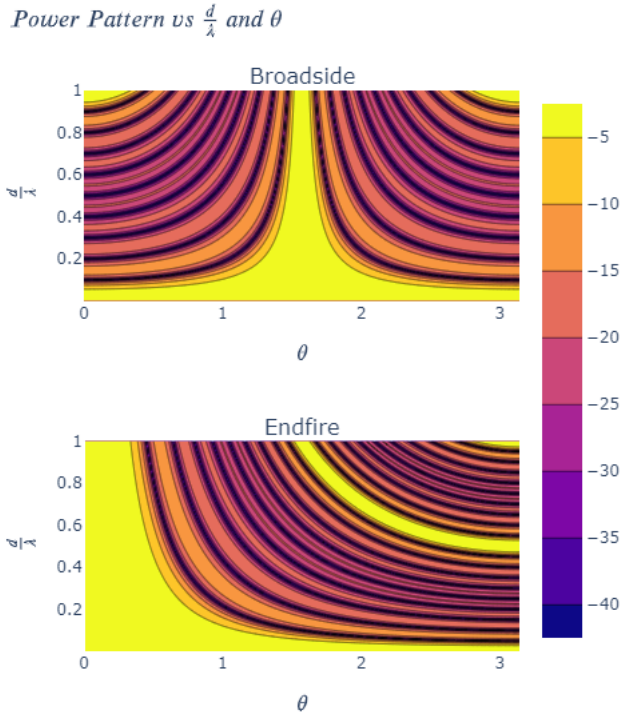

Figure 4: Power pattern vs θ and $\frac{d}{\lambda}$, broadside and endfire orientation.

Thus, for endfire orientation we get grating lobes when $\frac{d}{\lambda} \geq \frac{1}{2}$. For the broadside orientation, there are grating lobes when $\frac{d}{\lambda} \geq 1$, which it's out of the range for our case.

1.4

Now, the steering angles are $\theta \in \{0°, 30°, 60°, 90°\}$. From figure 5 we can list the next inferences:

1. For specific $\frac{d}{\lambda}$, the mainlobe width increases as steering angle decreases (we'll see more detailed plot in section 3.
2. As the $\frac{d}{\lambda}$ proportion increases, the grating lobes are more closer to the mainlobe.
3. For specific $\frac{d}{\lambda}$, as the steering angle is more smaller, the grating lobes are more close to the visible region.

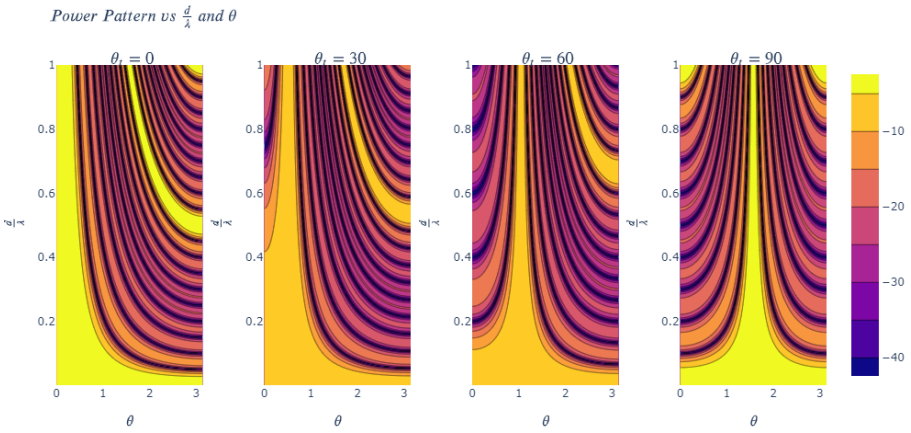

Figure 5: Power pattern vs θ and $\frac{d}{\lambda}$, various streering angles.

1.5

As we know (from equation (2)), the larger the number of sensors, the narrower the width of the main lobe. In addition, the value at the peak of the beam pattern decreases by $\frac{N}{N-N_{\text{number of failure sensors}}}$ as can be seen in figure 6. Thus, for $N = 10$ and 3 sensor failures the beanpatten amplitude decrease by $\frac{10}{3}$ (for the power pattern it's just squared) In addition, the nulls are no longer exactly zero, and the side lobes are greater.

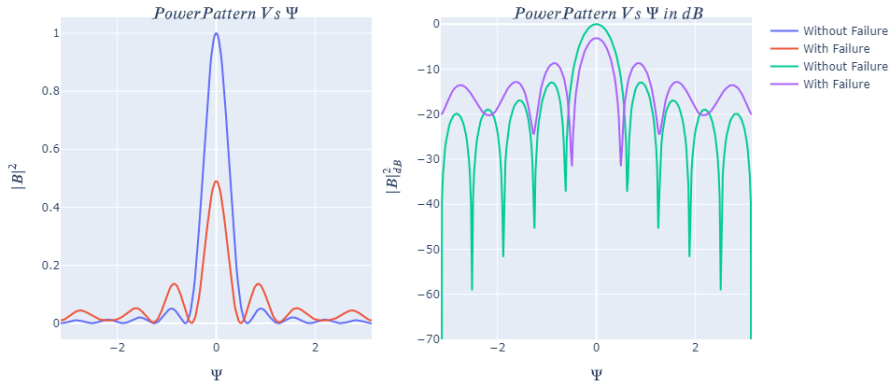

Figure 6: Power pattern vs ψ, with and without failure.

2 Non-uniform Weighting

In this section we examine the effect of the non-uniform weighting. In fact, this effect is exactly the effect of **filter design** with different types of windows. The reason for the similarity is because the beampattern is the Discrete-time Fourier transform (DTFT) of the sensors in the spatial i.e $B(\psi) = \sum_{m=0}^{N-1} w_m^* e^{jm\psi} = DTFT^*(w_m)$.

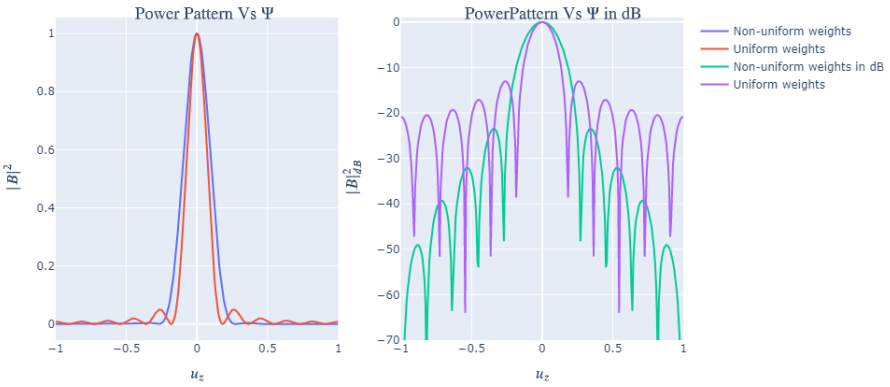

Figure 7: Power pattern vs u_z, with and without uniform weighting.

Hence, in figure 7, we can see that the main lobe is wider with non-uniform weighting, whereas the relative peak of the side lobe is greater in this case. In addition the null poisions are not the same

3 Half-Power Bandwidth

An ULA with N sensors is considered which is steered towards the direction Θ_t. The difference between the right and left half-power point is denoted by

$$\Theta_h = \Theta_r - \Theta_l.$$

(a) For $\Theta_t \notin \{0, \pm\pi\}$

$$\Theta_h \approx \frac{0.886\lambda}{Nd\sin\Theta_t}. \tag{4}$$

(b) For $\Theta_t \in \{0, \pm\pi\}$

$$\Theta_h \approx 2\sqrt{\frac{0.886\lambda}{Nd}}. \tag{5}$$

In this section we examine the half-power beamwidth (HPBW) for different steering angles. From figure 8 we can conclude the following:

- As we discussed, due to the non-linearity of the cos function, the main lobe width for the broadside configuration is changed according to (4). In addition, for the endfire configuration, the main lobe width behaves according to (5)
- For all the steering angles, as the ratio $\frac{Nd}{\lambda}$ increases, the mainlobe width decreases.
- For all $\frac{Nd}{\lambda}$ value, as the steering angle decreases the width of the main lobe becomes narrower.
-

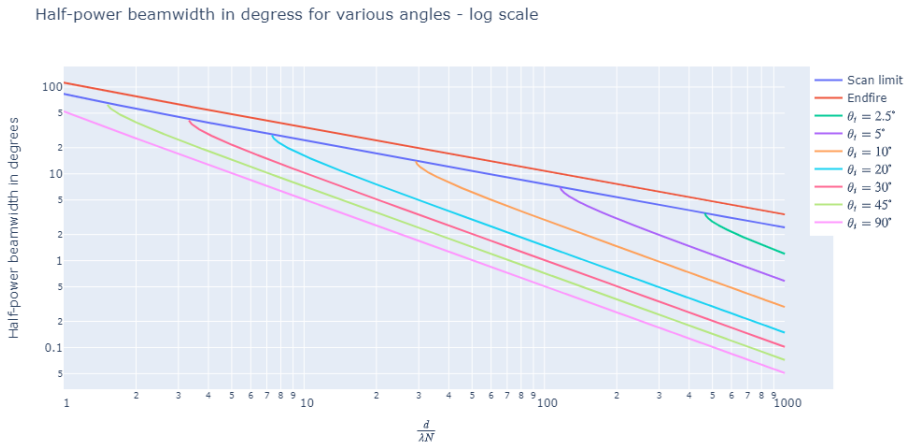

Figure 8: half-power beamwidth vs $\frac{Nd}{\lambda}$ for various steering angles.

4 Beampattern of MVDR Beamformer

4.1

In case of *INR=70dB*, the MVDR BF is the regular MVDR weights with following noise matrix:

$$\boldsymbol{S_n^{-1}} = \boldsymbol{P_1^{\perp}} = \boldsymbol{I} - \frac{\mathbf{1}}{\boldsymbol{N}} \frac{\mathbf{1}}{\boldsymbol{v_1 v_1^H}}$$

where the $\mathbf{P}_1^{\perp}$ is the orthogonal matrix to the interference's steering vector i.e $\boldsymbol{P_1^{\perp} v_1} = 0$. Thus, we expect to get $|B(u_{z_{interference}})|^2 = 0$ and $|B(u_{z_{desired}})|^2 = 1$, as can be seen in figures 9 and 10.

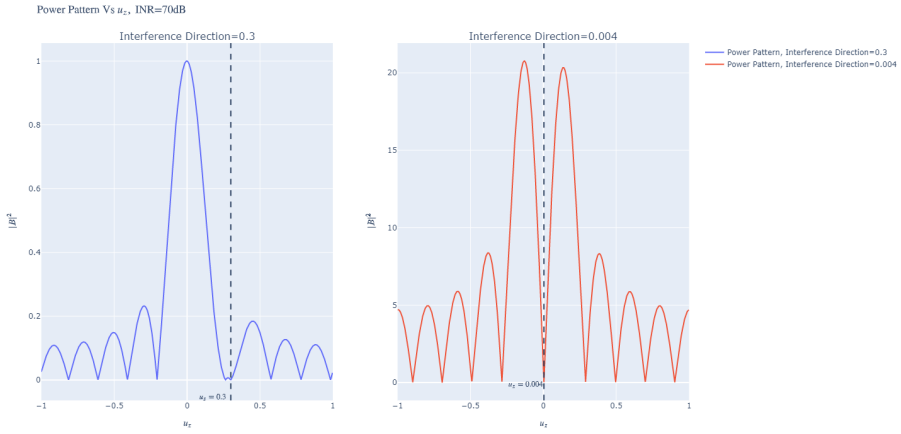

Figure 9: Powerpattern in u-domain, when the interference is located $u_z = 0.3$ and $u_z = 0.004$, *INR=70dB*.

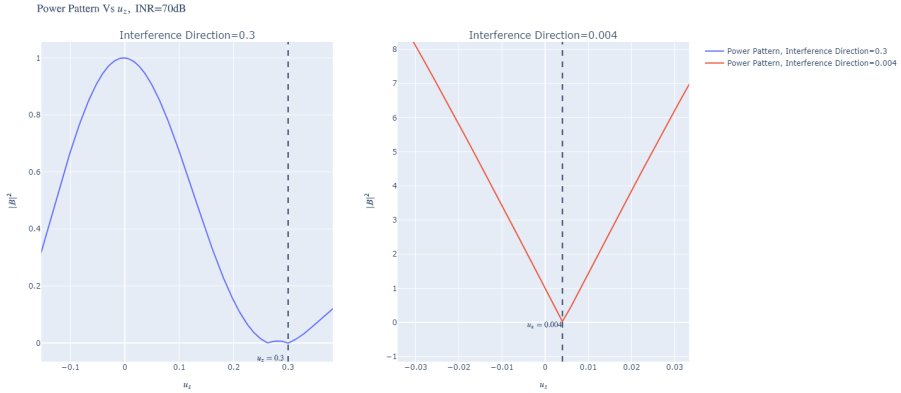

Figure 10: Powerpattern in u-domain, when the interference is located $u_z = 0.3$ and $u_z = 0.004$, *INR=70dB*, zoom-in.

However, in case of *INR=0dB*, the MVDR BF tries to minimize also the white noise, not only the directional noise. Hence, the ability of the BF to minimize the directional noise can be restricted, as it can be seen in figures 11 and 12

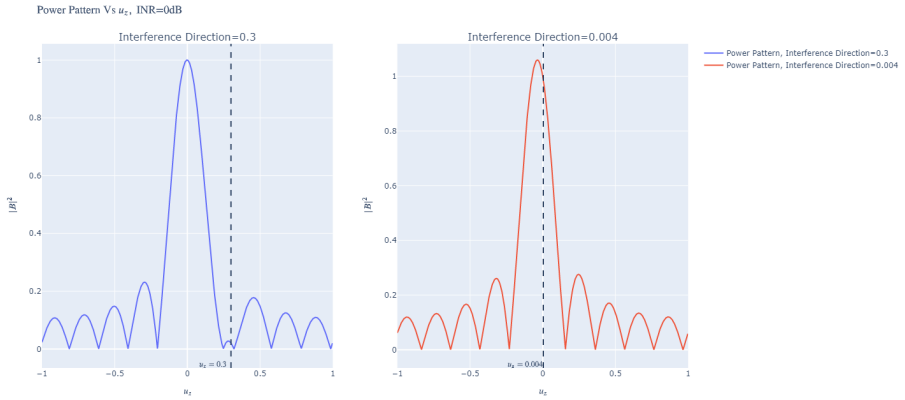

Figure 11: Powerpattern in u-domain, when the interference is located $u_z = 0.3$ and $u_z = 0.004$, *INR=0dB*.

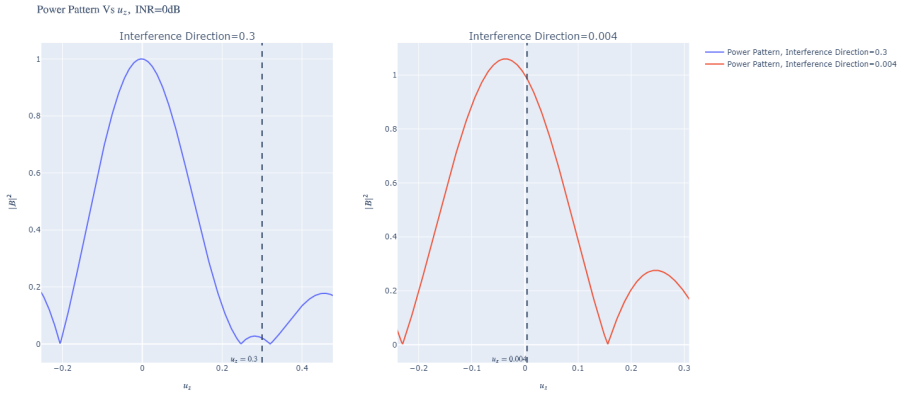

Figure 12: Powerpattern in u-domain, when the interference is located $u_z = 0.3$ and $u_z = 0.004$, *INR=0dB*, zoom-in.

More specific, in case of *INR=0dB*, if the interference is adjacent to the desired source, the beamformer barely filters it and more effort is expended to suppress the white noise

4.2

In this subsection we examine the powerpattern of the BF for interference located at $0.001 \leq u_1 \leq 0.5$. The figures 13 and 14 can confirm our explanation above.

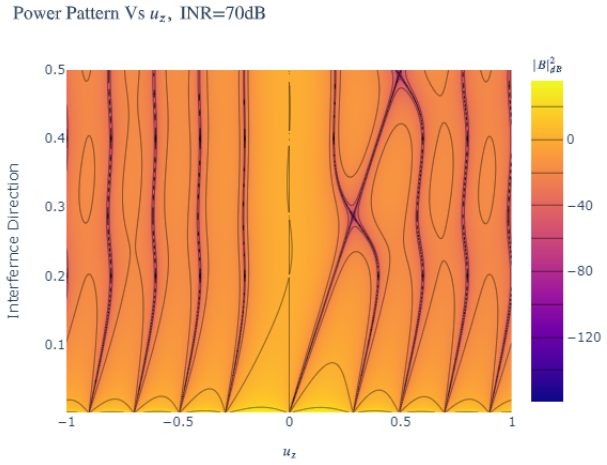

Figure 13: Powerpattern in u-domain for varying interfere directions, INR=70.

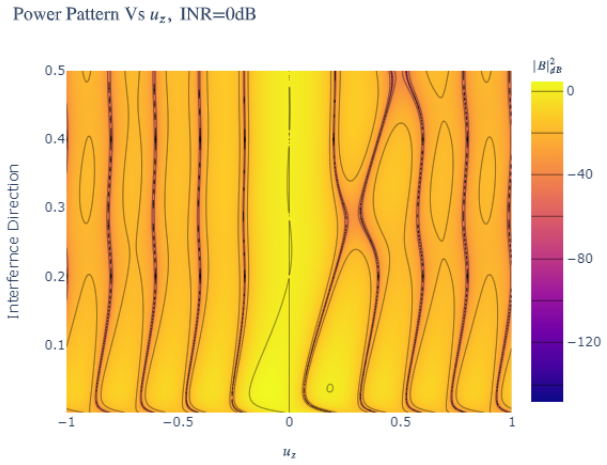

Figure 14: Powerpattern in u-domain for varying interfere directions, INR=0.

5 Delay-and-Sum Beamformer for Narrowband Signals

The behavior of the beamformer should be investigated by calculating the ratio of the input signal power to the output signal power of the beamformer (output-to-input ratio, OIR). In this section we consider an endfire and broadside orientation and different directions-of-arrival $\theta = 0°, 5°, \ldots, 90°$. In figure 15 we can see that the $OIR(\theta)$ fit the behavior of the delay-and-sum-beamformer(DSB): mainlobe width is more wider in the broadside than the endfire orientation. Note: we get $OIR_{endfire}(\theta) \leq 1$ in the endfire orientation, since in this orientation, the delay is maximial and in our algorithm the delayed values were replaced with zeros, so part of the signal's power lost. In addition, because of the characteristics of narrow-band signals, they do not occupy a single frequency like a monochromatic wave. As a result, the accuracy of the arrival difference offset is compromised. Accuracy is achieved only for the center frequency (carrier frequency) of the signal, not for the frequencies within the bandwidth of the signal. Examination of the resulting figures, it's evident that the calculated OIR resembles the beampattern of the DSB but exhibits distortion due to the inaccurate offset of the arrival difference.

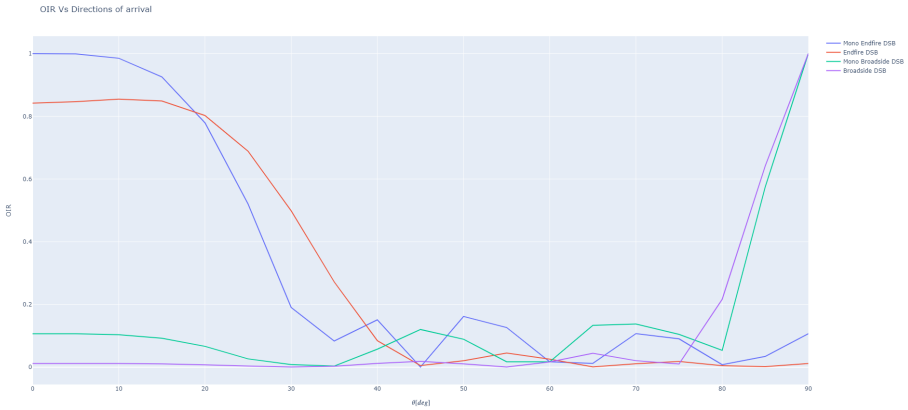

Figure 15: OIR vs θ.